Quaternary Science Reviews 197 (2018) 129–141

Contents lists available at ScienceDirect

Quaternary Science Reviews

journal homepage: www.elsevier.com/locate/quascirev

Beryllium-10 chronology of early and late Wisconsinan moraines in the Revelation Mountains, Alaska: Insights into the forcing of Wisconsinan glaciation in Beringia

Joseph P. Tulenko [a, *], Jason P. Briner [a], Nicolás E. Young [b], Joerg M. Schaefer [b]

[a] Department of Geology, University at Buffalo, Buffalo, NY, 14260, USA
[b] Lamont-Doherty Earth Observatory, Columbia University, Palisades, NY, USA

ARTICLE INFO

Article history:
Received 15 May 2018
Received in revised form
2 August 2018
Accepted 6 August 2018

Keywords:
Alaska
Late pleistocene
Wisconsinan glaciation
^{10}Be dating
Marine isotope stage 4
Moraines
Alpine glaciers

ABSTRACT

We present 32 new cosmogenic ^{10}Be exposure ages from a moraine sequence deposited during the Wisconsinan glaciation in the Swift River valley, Revelation Mountains, western Alaska Range. ^{10}Be ages from an early Wisconsinan [Marine Isotope Stage 4] moraine average 59.7 ± 3.6 ka (n = 9; excluding one outlier), and ^{10}Be ages from a late Wisconsinan [Marine Isotope Stage 2] terminal moraine, inboard moraines, and two recessional end moraines average 21.3 ± 0.8 ka (n = 3; excluding two outliers), 20.2 ± 1.0 ka (n = 7; excluding three young outliers), 19.6 ± 1.0 ka (n = 2; excluding one outlier) and 17.7 ± 0.8 ka (n = 4; excluding two outliers), respectively. The early Wisconsinan moraine age coincides with the close of MIS 4, consistent with previous chronologies from Beringia. Whereas Southern Hemisphere glaciers retreated prior to the onset of Heinrich Stadial 6 (64–60 ka), the MIS 4 glacier advance in the Swift River valley terminated at the close of Heinrich Stadial 6, possibly in response to abrupt North Atlantic warming. Our late Wisconsinan ages indicate significant initial glacier retreat between ca. 21.3–17.7 ka (prior to any significant increase in CO_2) likely in response to amplified warming from rising insolation. Preservation of MIS 4 moraines in Beringia has traditionally been ascribed to limited MIS 2 glacier advance modulated by low regional moisture availability, stemming from the exposed Bering Land Bridge. However, we hypothesize that atmospheric re-organization forced by the Laurentide Ice Sheet resulted in relatively higher temperatures and drier conditions in Beringia during MIS 2 than MIS 4, allowing for the preservation of early Wisconsinan moraines.

1. Introduction

Moraine sequences record the extent, timing and pace of mountain glacier advances and subsequent retreat. If precisely dated, chronologies from moraine sequences can give insight into the sensitivity of glaciers to global climate forcing and feedbacks [e.g. atmospheric CO_2, Shakun et al. (2012); polar amplification of temperature change, Miller et al. (2010)]. While extensive effort has been spent to constrain interhemispheric links between global climate forcing and glacier retreat following the Last Glacial Maximum (LGM, 26–19 ka; Clark et al., 2009), these linkages are generally restricted to alpine glaciers in the mid-to-low-latitudes as these regions were not covered by continental ice sheets (Schaefer et al., 2006; Shakun et al., 2015). Moreover, due primarily to poor moraine preservation and limitations to dating techniques for moraines older than the last deglaciation, knowledge of glacier behavior over multiple glacier advances is particularly sparse. While alpine glaciers in the mid-to-low-latitudes may have synchronously retreated in response to global climate forcing (e.g., rising CO_2 concentrations) during the last deglaciation (Shakun et al., 2012, 2015), there are relatively few records available to evaluate whether or not the same is true for the high northern latitude glaciers (e.g., Briner et al., 2017), nor are there enough records to evaluate whether the synchronicity between glacier retreat and CO_2 forcing persisted through multiple glacial cycles (e.g., Schaefer et al., 2015).

Beringia provides an opportunity to study alpine-style glaciation in the high northern latitudes. Among the high northern latitudes, interior regions of Beringia remained some of the only locations never occupied by late Pleistocene continental ice sheets

* Corresponding author.
E-mail address: jptulenk@buffalo.edu (J.P. Tulenko).

https://doi.org/10.1016/j.quascirev.2018.08.009
0277-3791/

(Fig. 1). Glaciation over many cycles was instead restricted to high mountain centers in the region (Kaufman et al., 2011, Fig. 1). In addition, since much of Alaska remained ice-free throughout the late Pleistocene, and LGM ice was relatively limited in extent, moraine sequences from pre-LGM glacier advances are preserved on the landscape (Briner et al., 2005; Kaufman et al., 2011). Previous attempts at dating pre-LGM moraines in a few sites in Beringia have loosely constrained the penultimate ice advance to Marine Isotope Stage 4 (MIS 4, e.g. Briner et al., 2001, 2005; Brigham-Grette et al., 2003; Ward et al., 2007; Dortch et al., 2010; Turner et al., 2013). However, ages from these studies are few and chronologically scattered, making it difficult to assess how the timing of regional deglaciation relates to changes in various climatic forcing mechanisms and feedbacks during the MIS 4 – MIS 3 transition.

Combining detailed moraine mapping with cosmogenic ^{10}Be exposure dating (hereafter referred to as ^{10}Be dating), we build on a survey of Briner et al. (2005), who sampled granitic boulders embedded in left lateral moraines lining the Swift River valley (61.5° N, 154.5° W) that dated from early MIS 3 to MIS 2. We provide 32 new ^{10}Be ages that: 1) constrain the culmination of early Wisconsinan [MIS 4] glacier advance in the Swift River valley, and 2) provide a record of initial retreat in the Swift River valley following late Wisconsinan [MIS 2] glacier advance. With our updated chronology, we review and discuss possible mechanisms that led to the pattern of Wisconsinan glaciation observed in Beringia.

2. Background

During the late Pleistocene, the northwestern extension of the Cordilleran Ice Sheet occupied southern Alaska and much of the Yukon, but local ice fields and valley glaciers existed in the Brooks Range, interior-facing slopes of the Alaska Range, the Ahklun Mountains and in several other smaller mountainous areas throughout Beringia (Kaufman et al., 2011, Fig. 1). This left much of Beringia ice-free during the late Pleistocene. Based on radiocarbon ages ranging from 24 to 11 ka of glacial deposits in locations that were either occupied by local ice or near the maximum limit of the Cordilleran Ice Sheet, the most recent glaciation in Beringia was similar in age to late Wisconsinan [MIS 2] glaciation elsewhere in North America (Porter et al., 1983; Hamilton et al., 1986; Hamilton, 1994; Sheinkman, 2011). Whereas the penultimate glaciation in other parts of North America is constrained to MIS 6 [e.g., Bull Lake glaciation; Pierce (2003)], moraines deposited directly outboard of late Wisconsinan moraines in a few sites in Beringia have been assigned to MIS 4 or early MIS 3 (e.g., Brigham-Grette et al., 2003; Briner et al., 2005; Ward et al., 2007; Dortch et al., 2010) with the notable exception of deposits associated with the Selwyn Lobe of the CIS (Ward et al., 2008). While there are many studies that constrain the age of pre-MIS 2 and MIS 2 terminal alpine glacier moraines in Beringia (Brigham-Grette et al., 2003; Briner et al., 2005, 2017; Kaufman et al., 2011), no detailed record of an entire alpine glacier moraine sequence spanning the Wisconsinan glaciation from a single valley yet exists in the region. All ^{10}Be ages reviewed in this section are re-calculated; see methods.

2.1. Wisconsinan moraine ages in Beringia

Alpine glaciers deposited well-preserved moraine sequences in many valleys along the northern and western Alaska Range front (Fig. 2). In the northeastern range front, Young et al. (2009) obtained an average ^{10}Be age of 18.7 ± 0.1 ka (n = 4; excluding one old outlier and two young outliers) for a late Wisconsinan moraine and concluded that ice may have remained at or near its maximum late Wisconsinan position for a few thousand years before rapidly retreating. In the Donnelly Dome region, ^{10}Be ages from a late Wisconsinan terminal moraine average 19.1 ± 0.8 ka (n = 6; excluding two old outliers and three young outliers; Matmon et al., 2010). In the central Alaska Range, Dortch et al. (2010) sampled boulders for ^{10}Be dating at multiple locations, including drift from the pre-late Wisconsinan Healy advance. They report an average age of 58.7 ± 4.0 ka (n = 8; excluding one young outlier). Dortch et al. (2010) also report ages from drift of the Riley Creek advance and the Carlo Creek re-advance, which were both previously mapped as late Wisconsinan (Wahrhaftig and Black, 1958). The Riley Creek advance is likely the maximum late Wisconsinan extent, but ages are scattered (ranging from ca. 1–61 ka) and difficult to interpret; however, the Riley Creek advance must be older than the Carlo Creek re-advance, which is dated to 18.7 ± 0.7 ka (n = 5; excluding two young outliers and one old outlier).

Perhaps the most complete chronology of glacier retreat spanning the last deglaciation in the northern Alaska Range is from Denali National Park. Ten Brink and Waythomas (1985) mapped

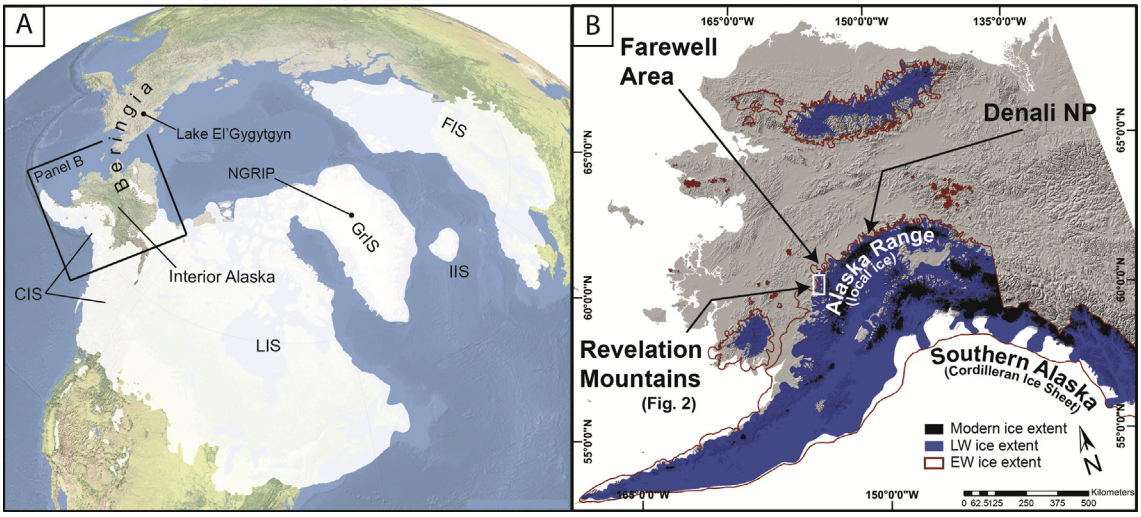

Fig. 1. A) Limits of LGM glaciation in the Northern Hemisphere [Laurentide (LIS), Cordilleran (CIS), Greenland (GrIS), and Icelandic (IIS) ice sheets from Dyke (2004) and Fennoscandian Ice Sheet (FIS) from Hughes et al. (2016)] and locations of Lake El'Gygytgyn and the NGRIP drill site. B) Limits of LGM and early Wisconsinan glaciation in Alaska (Kaufman et al., 2011).

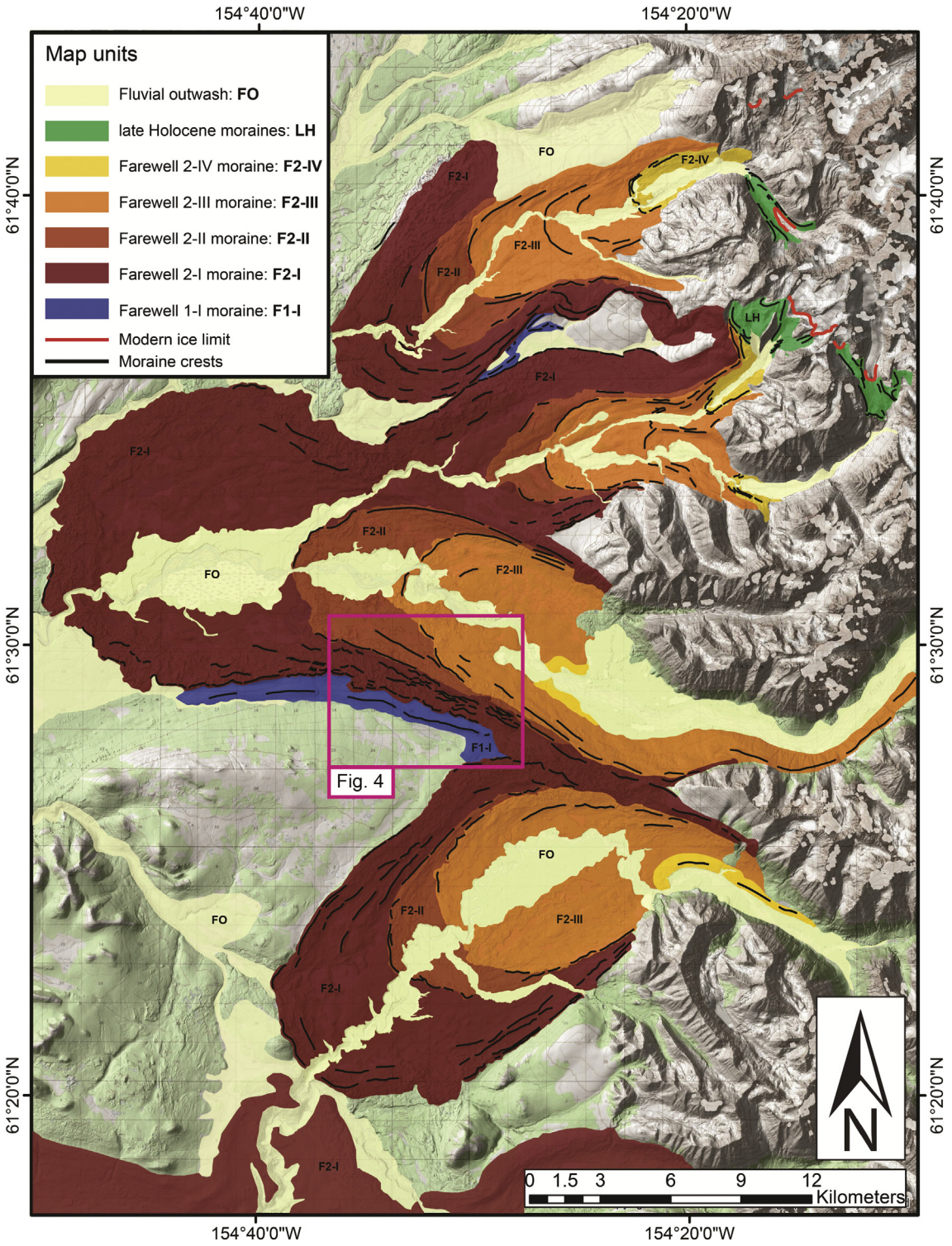

Fig. 2. Distribution of moraines in the western Revelation mountains. Topographic base map available online from ArcGIS online, and 2-m horizontal resolution hillshade relief map downloaded from the PGC's ArcticDEM website (http://www.pgc.umn.edu/arcticdem). Map units in inset legend.

and dated glacial deposits from the locally termed McKinley Park (MP) glaciation, a four-fold late Wisconsinan moraine sequence. Radiocarbon ages of organic material situated above and below drift of the maximum late Wisconsinan advance (MP-I) constrain the timing of deposition between 23.7 ± 0.5 and 21.5 ± 0.8 cal kyr BP. Werner et al. (1993) and Child (1995) constrained two of the remaining glacial advances (MP-II and MP-III) with deposits from sediment cores and bluff exposures collected at Wonder Lake. Based on radiocarbon ages, the MP-II advance is constrained between 20.7 ± 0.4 and 17.1 ± 0.5 cal kyr BP and the MP-III advance is constrained between 15.1 ± 0.7 and 14.6 ± 0.5 cal kyr BP. The final late Wisconsinan advance (MP-IV) dates between 12.1 ± 0.5 and 11.5 ± 0.4 cal kyr BP based on radiocarbon ages that date the initial formation of peat in front of, and on, the MP-IV end moraine. The

four-fold sequence of late Wisconsinan moraines observed in Denali National Park is consistent with sequences found in most valleys along the northern and western slopes of the Alaska Range (Kaufman and Manley, 2004).

Beyond the Alaska Range, some key alpine galcier chronologies add to the framework of Wisconsinan glacier history in Beringia. In the Brooks Range, ^{10}Be ages constrain the early Wisconsinan phase (locally termed the Itkillik I glaciation) to MIS 4/3, and the culmination of the late Wisconsinan advance at 25.5 ± 3.1 ka in the northeast Brooks Range and 21.4 ± 1.6 ka in the north-central Brooks Range (Balascio et al., 2005; Pendleton et al., 2015). In the Ahklun Mountains, which were occupied by a local ice cap, multiple studies provide a detailed reconstruction of Wisconsinan glaciation. Briner et al. (2001) used ^{36}Cl ages to determine that the early Wisconsinan advance culminated at 58.3 ± 2.3 ka (ages recalculated using version 2.0 of the CRONUS Earth Web Calculator; http://cronus.cosmogenicnuclides.rocks/2.0/). In addition, radiocarbon constraints from glaciolacustrine sediments in Arolik Lake sediment cores indicate that the late Wisconsinan maximum advance culminated between 23.9 and 19.1 cal kyr BP (Kaufman et al., 2003, 2012); one recessional moraine was emplaced no later than 20.4 ± 0.3 cal kyr BP (Manley et al., 2001).

Few other regions in Beringia outside of the prominent Alaskan mountain ranges provide chronologic constraints on Wisconsinan moraines. In eastern Beringia, Ward et al. (2007) dated drift related to an early Wisconsinan advance of the Cordilleran Ice Sheet in the Yukon Territory at 55.0 ± 1.5 ka (n = 4), which is loosely matched with ages from an alpine glacier further west in the Yukon Tanana Upland that range between 60 and 40 ka (Briner et al., 2005). In western Beringia, ^{36}Cl ages from alpine glacier moraines in the Pekulney Mountains also broadly constrain the early Wisconsinan advance between 70 and 40 ka (Brigham-Grette et al., 2003). Despite a large degree of scatter in ^{36}Cl ages on late Wisconsinan moraines in the same region, the observed pattern of subdued late Wisconsinan advance in western Beringia is consistent with central and eastern Beringia (Brigham-Grette et al., 2003).

2.2. The Revelation Mountains field site

West of Denali National Park, alpine glaciers deposited extensive moraine sequences during the locally termed Farewell glaciation (Fernald, 1953). Kline and Bundtzen (1986) describe the two main phases of the Farewell glaciation, suggesting that Farewell-I was early Wisconsinan [MIS 4] in age and that the Farewell-II advance was analogous to the McKinley Park glaciation [MIS 2]. Here, we focus on the Revelation Mountains, wherein alpine glaciers deposited numerous moraine sequences during the Farewell glaciation (Fig. 2). Moraines in the Swift River valley (Figs. 2 and 4) contain abundant large, quartz bearing granitic boulders from the McKinley sequence, which comprises much of the Revelation Mountains (Lanphere and Reed, 1985). Briner et al. (2005) sampled four boulders on moraines of the maximum Farewell-II drift (map unit: F2-I) averaging 20.4 ± 0.7 ka, and four boulders from a Farewell-I moraine (map unit: F1-I) averaging 52.7 ± 5.1 ka.

Over a decade of progress in ^{10}Be extraction procedures and analytical measurements spurred our interest in improving and extending the chronology of Briner et al. (2005). In addition to resampling early and late Wisconsinan terminal moraines in the Swift River valley, we dated boulders on two recessional moraines inboard of the early and late Wisconsinan terminal moraines. The moraine sequence continues up valley, but we did not sample any moraines deposited beyond the second recessional moraine (F2-III; Fig. 2). The present ice margin is ca. 56 km up valley from the maximum MIS 2 moraine in Swift River Valley; a series of likely Holocene moraines occur just beyond the present glacier terminus.

3. Methods

3.1. Moraine mapping

Using the Polar Geospatial Center's ArcticDEM (http://www.pgc.umn.edu/arcticdem), which provides complete coverage of the study area with digital topographic data at 2-m horizontal resolution, we digitized moraine units and made interpretations on hillshade renders with 4x vertical exaggeration. We traced prominent moraine crests and subdivided the landscape into seven age units according to their stratigraphic order: 1) early Wisconsinan [MIS 4] lateral moraines (F1-I), 2) the outermost late Wisconsinan [MIS 2] moraine crest and inboard ground moraines (F2-I), 3–5) three late Wisconsinan recessional moraine crests and their inboard ground moraines (F2-II-IV), 6) late Holocene moraines (LH), and 7) alluvium units that dissect the moraines (FO; Fig. 2). We relied on both moraine morphology and previous age control for unambiguous distinction between early and late Wisconsinan units on the map. However, we initially relied solely on moraine morphology to distinguish the four fold late Wisconsinan sequence that is also observed in most other valleys across the nothern Alaska Range (Kaufman and Manley, 2004). F2-II, F2-III and F2-IV recessional moraines were identified by their continuous, sharp crested outer limits and hummocky terrain immediately inboard. We also calculated centerline distances between the recessional moraine units and found consistency throughout each of the valleys we mapped.

3.2. Sample collection, processing and AMS measurements

Guided by our moraine mapping, we dated 32 large, tabular, granitic boulders embedded in moraine crests; 10 boulders on the F1-I lateral moraine, five boulders on the outermost F2-I lateral moraine crest, eight boulders on discontinuous moraines within the F2-I unit, three boulders on a moraine within the F2-II limit, and six boulders on the outermost moraine of the F2-III unit (Fig. 3; Table 1). We sampled the top few centimetres of each boulder with a battery-powered angle grinder rock saw paired with a hammer and chisel, extracting ca.1–2 kg of sample per boulder (Fig. 3). To minimize the influence of erosion, we sampled smooth, low-sloping surfaces and avoided weathering pits, which were rare on Farewell-II boulders and more common on Farewell-I boulders. Sampled boulders were selected based on field observations; we chose only large boulders directly on moraine crests that exhibited minimal evidence of post-depositional movement. We took GPS and elevation data for each sample using a handheld GPS device (Table 1). We did not measure significant (>5°) topographic shielding at any of the sampled boulders.

All samples were prepared for ^{10}Be analysis at the University at Buffalo Cosmogenic Nuclide Laboratory following a slightly modified procedure from Kohl and Nishiizumi (1992). Each sample was crushed and sieved, and quartz-rich fractions were separated using a froth flotation method. Quartz fractions were then purified by a sequence of dilute HF/HNO_3 etches. Sample aliquots were tested for quartz purity via ICP-AES analysis at the Laboratory for Environmental and Geological Studies, University of Colorado, Boulder. Two sample batches consisted of 11 samples and a process blank for the late Wisconsinan samples, and one batch consisted of 10 samples and a process blank for the early Wisconsinan samples. Beryllium isolation procedures followed a slightly modified version of the method developed at the University of Vermont (Corbett et al., 2016). ^{10}Be/^{9}Be ratios for each sample were measured at the Center for Accelerated Mass Spectrometry, Lawrence Livermore National Laboratory. All samples were normalized to the 07KNSTD3110 standard with a reported ratio of 2.85×10^{-12}

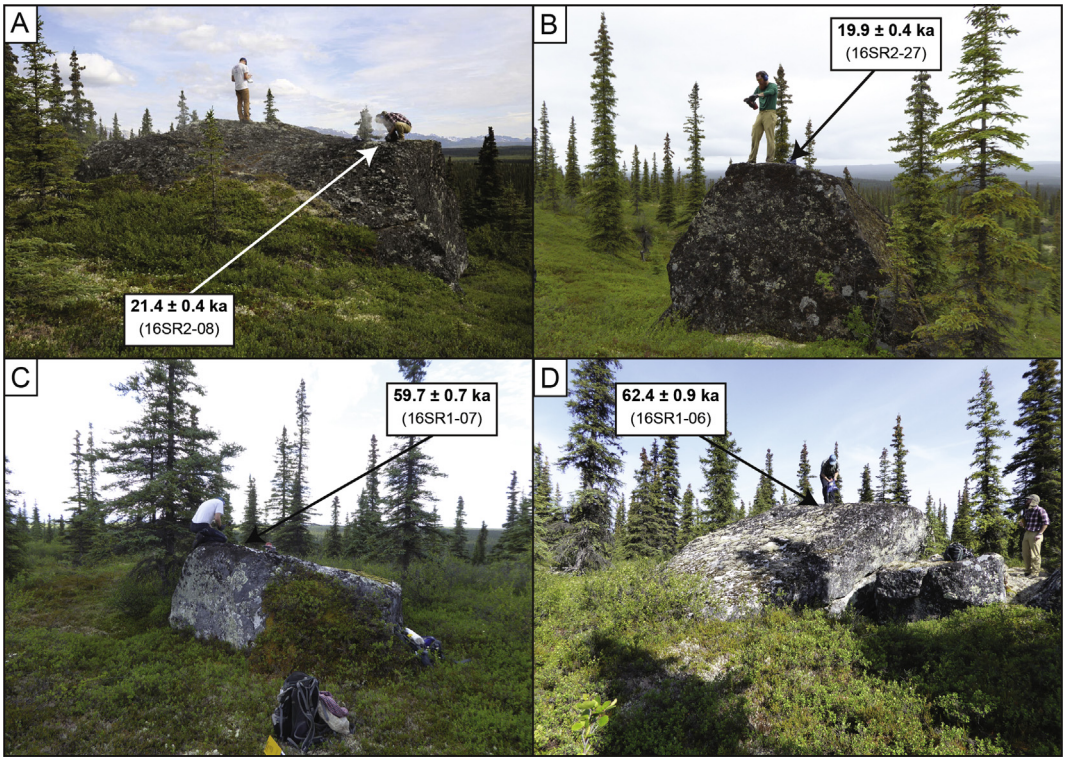

Fig. 3. Examples of boulders sampled for ^{10}Be dating (see supplement for more examples). A) 16SR2-08 (21.4 ± 0.4 ka), collected from the outermost F2-I moraine. B) 16SR2-27 (19.9 ± 0.4 ka) collected on a moraine just outboard of the F2-III outermost moraine. C,D) 16SR1-07 and 16SR1-06 (59.7 ± 0.7 ka and 62.4 ± 0.9 ka, respectively) both collected on the crest of the F1-I moraine.

(Nishiizumi et al., 2007). Process blank ratios were 3.63×10^{-15}, 4.23×10^{-15}, and 3.98×10^{-14}. Sample uncertainties are reported as 1-sigma internal AMS uncertainties and range from 1.2 to 2.9% (Table 1).

3.3. ^{10}Be age calculations

We calculated all ^{10}Be ages (including those previously mentioned from other studies in Alaska) using the CRONUS-Earth online calculator (developmental version 3; http://hess.ess.washington.edu/math/; Table 1) using Lm scaling (Lal, 1991/Stone, 2000) and the Arctic production rate of Young et al. (2013). This production rate calibration is applied to ^{10}Be ages from sites in Beringia (Margold et al., 2014; Pendleton et al., 2015) and is comparable to other regional production rates (e.g. Balco et al., 2009). We note that the Arctic rate of Young et al. (2013) is slightly lower than the Scandinavian rate of Stroeven et al. (2015), but thus far it is what has been applied in Beringia. Ages from this study, calculated using alternative production rates and scaling factors, can be seen in Table 1. Without knowing what erosion rate to apply, we present ages with a zero erosion rate. Because sampled boulders were large and on ridge tops that we assume have been adequately windswept of snow, we assume that there is no significant snow shielding that affected boulder surface inventories. Thus, ages presented here are minimum exposure ages.

We subdivided our ^{10}Be ages into five morphostratigraphic units based on mapping, which includes a distinction between the continuous F2-I outermost crest and discontinuous crests situated between the continuous F2-I and F2-II outermost crests (Figs. 4 and 5). We first calculated χ^2 values at 95% confidence to identify whether ages from each unit are normally distributed and representative of one single event (i.e., the timing of moraine emplacement). Then, we systematically identified and removed potential outliers using Chauvenet's Criterion, and re-calculated the average, standard deviation and χ^2 values for each unit (Fig. 5). Unit age uncertainties reported here include one standard deviation with a ^{10}Be production rate uncertainty of 3.7% propagated through (Young et al., 2013). For the boulders that we re-sampled, we calculate their ^{10}Be age by taking the average between the pilot age and the new age as long as the new age is reproduced within error of the pilot age.

4. Results

4.1. Moraines

Each mapped valley displays the typical four-fold late Wisconsinan [MIS 2] sequence observed by Kaufman and Manley, 2004, yet some contain multiple smaller moraines preserved among the four main units. In addition, we identified early Wisconsinan [MIS 4] lateral moraines in two of the valleys, and in a few valleys mapped moraines found slightly outboard of modern ice that are likely late Holocene in age (Fig. 2). Ground truthing supported mapping observations, and revealed notable contrasts between the early and late Wisconsinan moraines. The early Wisconsinan moraine is subdued, with a maximum relief of 10 m. Boulders on the moraine commonly contained large weathering pits, which we avoided, but exhibited little frost-shattering. Conversely, late Wisconsinan moraines measure between 20 and 25 m in height, and display sharp, continuous crests at the maximum extent and two recessional extents. Inboard of each continuous crest, we observed hummocky terrain containing a series of discontinuous crests. Weathering pits were not common on late Wisconsinan moraine boulders, but we observed evidence of significant frost-shattering on some boulders,

Table 1
Sample data and ^{10}Be ages.

Sample Name	Latitude	Longitude	Elevation	Thickness	Boulder	Quartz	^{9}Be	^{10}Be concentration	^{10}Be age	^{10}Be age	^{10}Be age
	(DD)	(DD)	(m asl)	(cm)	Height (m)	(g)	(μg)	(atoms/g)	(ka)[a]	(ka)[b]	(ka)[c]
Farewell1-I MIS 4 moraine											
16SR1-01	61.47381	−154.54	568	2.0	2.0	36.04	230	441166 ± 8213	60.1 ± 1.1	61.8 ± 1.2	56.5 ± 1.1
16SR1-02	61.47426	−154.543	569	2.0	2.5	30.20	231	463067 ± 6148	63.1 ± 0.9	64.8 ± 0.9	59.2 ± 0.8
16SR1-05	61.47673	−154.556	557	2.0	3.5	30.09	230	414049 ± 5141	56.9 ± 0.7	58.5 ± 0.7	53.5 ± 0.7
16SR1-06	61.48068	−154.583	545	2.0	3.0	24.51	232	428981 ± 5269	59.7 ± 0.7	61.3 ± 0.8	56.1 ± 0.7
16SR1-07	61.47031	−154.507	599	1.0	1.8	36.26	233	474565 ± 6649	62.4 ± 0.9	64.1 ± 0.9	58.6 ± 0.8
16SR1-08	61.47004	−154.503	602	2.0	1.5	42.14	228	427689 ± 5900	56.4 ± 0.8	58.0 ± 0.8	53.0 ± 0.7
16SR1-09	61.46986	−154.503	618	1.0	2.5	35.33	231	409057 ± 5730	52.7 ± 0.7	54.2 ± 0.8	49.5 ± 0.7
16SR1-10	61.46981	−154.501	611	2.0	2.5	22.08	231	428753 ± 6184	56.1 ± 0.8	57.6 ± 0.8	52.7 ± 0.8
16SR1-11	61.46777	−154.489	627	2.0	2.0	40.13	229	483457 ± 7166	62.4 ± 0.9	64.1 ± 1.0	58.6 ± 0.9
16SR1-12	61.46767	−154.49	617	1.0	4.0	42.53	231	481266 ± 6645	62.2 ± 0.9	63.9 ± 0.9	58.4 ± 0.8
Farewell2-I MIS 2 outermost moraine											
16SR2-03	61.47854	−154.534	613	2.0	3.0	16.19	232	137461 ± 3436	17.8 ± 0.4	18.3 ± 0.5	16.8 ± 0.4
16SR2-04	61.49005	−154.597	578	2.0	1.5	14.42	216	183188 ± 4087	24.5 ± 0.6	25.2 ± 0.6	23.1 ± 0.5
16SR2-06	61.48498	−154.573	579	2.5	2.5	13.39	180	158819 ± 4311	21.3 ± 0.6	21.9 ± 0.6	20.1 ± 0.5
16SR2-08	61.48217	−154.556	600	2.0	2.0	12.15	230	162740 ± 3240	21.4 ± 0.4	22.0 ± 0.4	20.1 ± 0.4
16SR2-09	61.4818	−154.553	598	3.0	2.0	15.78	199	159922 ± 3081	21.2 ± 0.4	21.8 ± 0.4	19.9 ± 0.4
Farewell2-I MIS 2 inner moraines											
16SR2-02	61.48095	−154.535	600	2.0	3.0	13.71	248	155077 ± 3230	20.3 ± 0.4	20.9 ± 0.4	19.1 ± 0.4
16SR2-05	61.48576	−154.575	579	2.0	1.5	12.27	227	125224 ± 2836	16.7 ± 0.4	17.2 ± 0.4	15.8 ± 0.4
16SR2-07	61.48565	−154.567	588	2.0	1.5	15.31	227	141861 ± 2742	18.8 ± 0.4	19.4 ± 0.4	17.7 ± 0.3
16SR2-12	61.4845	−154.551	584	2.0	2.0	12.05	226	147499 ± 2879	19.6 ± 0.4	20.2 ± 0.4	18.5 ± 0.4
16SR2-13	61.48392	−154.551	585	2.0	2.0	13.51	226	151940 ± 2944	20.2 ± 0.4	20.8 ± 0.4	19.0 ± 0.4
16SR2-16	61.49388	−154.575	531	3.0	2.5	13.13	226	106121 ± 2120	15.0 ± 0.3	15.4 ± 0.3	14.1 ± 0.3
16SR2-18	61.48802	−154.548	556	2.0	2.5	12.39	225	99883 ± 2113	13.6 ± 0.3	14.0 ± 0.3	12.8 ± 0.3
16SR2-19	61.48323	−154.528	589	2.0	3.0	20.26	226	163025 ± 4753	21.6 ± 0.6	22.2 ± 0.7	20.3 ± 0.6
Farewell2-II first recessional moraine											
16SR2-22	61.49344	−154.527	457	2.0	1.5	20.44	225	180016 ± 4913	27.0 ± 0.7	27.7 ± 0.8	25.4 ± 0.7
16SR2-23	61.4938	−154.527	454	2.0	2.0	20.30	226	127099 ± 2797	19.1 ± 0.4	19.6 ± 0.4	18.0 ± 0.4
16SR2-27	61.49131	−154.522	487	2.0	3.0	20.33	225	137156 ± 2635	20.0 ± 0.4	20.5 ± 0.4	18.8 ± 0.4
Farewell2-III second recessional moraine											
16SR2-24	61.49681	−154.528	443	2.0	1.8	20.92	230	116621 ± 2268	17.7 ± 0.3	18.2 ± 0.4	16.7 ± 0.3
16SR2-25	61.49519	−154.526	461	1.5	1.5	19.68	201	116619 ± 2263	17.3 ± 0.3	17.8 ± 0.3	16.3 ± 0.3
16SR2-28	61.492	−154.519	476	2.0	1.8	19.48	204	118171 ± 2293	17.4 ± 0.3	17.9 ± 0.3	16.4 ± 0.3
16SR2-29	61.49027	−154.514	477	1.0	2.0	20.20	230	193215 ± 3387	28.2 ± 0.5	29.0 ± 0.5	26.5 ± 0.5
16SR2-30	61.49023	−154.513	484	1.0	1.8	15.60	230	170165 ± 4622	24.7 ± 0.7	25.4 ± 0.7	23.2 ± 0.6
16SR2-31	61.48983	−154.511	486	2.0	2.5	20.57	229	126715 ± 2124	18.5 ± 0.3	19.0 ± 0.3	17.4 ± 0.3

Notes: Rock density for all samples 2.65 g/cm^3; zero boulder surface erosion rate applied to all samples; no shielding correction applied to all samples.
[a] All ages calculated using the Arctic production rate (Young et al., 2013) and Lm scaling (Lal, 1991/Stone, 2000).
[b] All ages calculated using the Arctic production rate (Young et al., 2013) and LSD scaling (Lifton et al., 2014a).
[c] All ages calculated using the Cronus default production rate (Borchers et al., 2016) and LSD scaling (Lifton et al., 2014a).

which we avoided.

Additionally, we measured glacier length changes along centerlines in each valley. In the Swift River valley, the innermost recessional moraine that we dated (F2-III) has its end moraine positioned ca. 14 km up valley of the F2-I terminal moraine. With the modern ice limit ca. 56 km up valley from the F2-I terminal moraine, we calculate a ca. 25% reduction in glacier length between the two measured positions. We made the same measurements for the three other mapped valleys and find length reductions that were comparable (ranging from ca. 20–30%).

4.2. ^{10}Be ages

Eleven ^{10}Be ages from the Farewell-I moraine (including three ages from the pilot study) range from 63.1 ± 0.9 to 56.1 ± 0.8 ka, with two younger outliers at 52.7 ± 0.7 ka and 50.8 ± 1.7 ka (Table 1). Excluding the two outliers, nine ages average 59.7 ± 3.6 ka. The 22 remaining ^{10}Be ages on Farewell-II moraines range from 28.2 ± 0.5 ka to 13.6 ± 0.3 ka (Fig. 4; Table 1). We split these moraines into four morphostratigraphic units, and present the ages from oldest to youngest unit. Along the outermost, terminal Farewell-II moraine crest (F2-I), five ages range from 24.5 ± 0.6 to 17.8 ± 0.4 ka. Of those, three ages are nearly identical, averaging 21.3 ± 0.8 ka. Inboard of the outermost F2-I moraine crest, we dated eight boulders from discontinuous moraine crests within the F2-I limit and outboard of the F2-II liimit. The new ages, along with four ages from the pilot study, range from 21.6 ± 0.6 ka to 13.6 ± 0.3 ka, and the three youngest ages do not statistically overlap. However, the seven remaining ages all statistically overlap, averaging 20.2 ± 1.0 ka. We dated three boulders on a crest within the first prominent recessional moraine unit (F2-II). Ages range from 27.0 ± 0.7 ka to 19.1 ± 0.4 ka. Whereas one age is older, the remaining two ages statistically overlap, averaging 19.6 ± 1.0 ka. Finally, on the second recessional moraine that we dated (F2-III), six ages range from 28.2 ± 0.5 to 17.3 ± 0.3. Two older ages show a wide spread, and do not statistically overlap. The remaining four ages from the F2-III crest average 17.7 ± 0.8 ka. Thus, after accounting for outliers, our moraine ages are in stratigraphic order.

5. Discussion

5.1. Moraine stability and reliability of the ^{10}Be chronology

Post-depositional boulder exhumation and overturning resulting from moraine degradation leads to scattered and erroneously young ^{10}Be ages (Putkonen and Swanson, 2003; Putkonen et al., 2008). This presents a concern in Alaska, where many moraines were likely ice-cored when deposited (Briner et al., 2005; Young

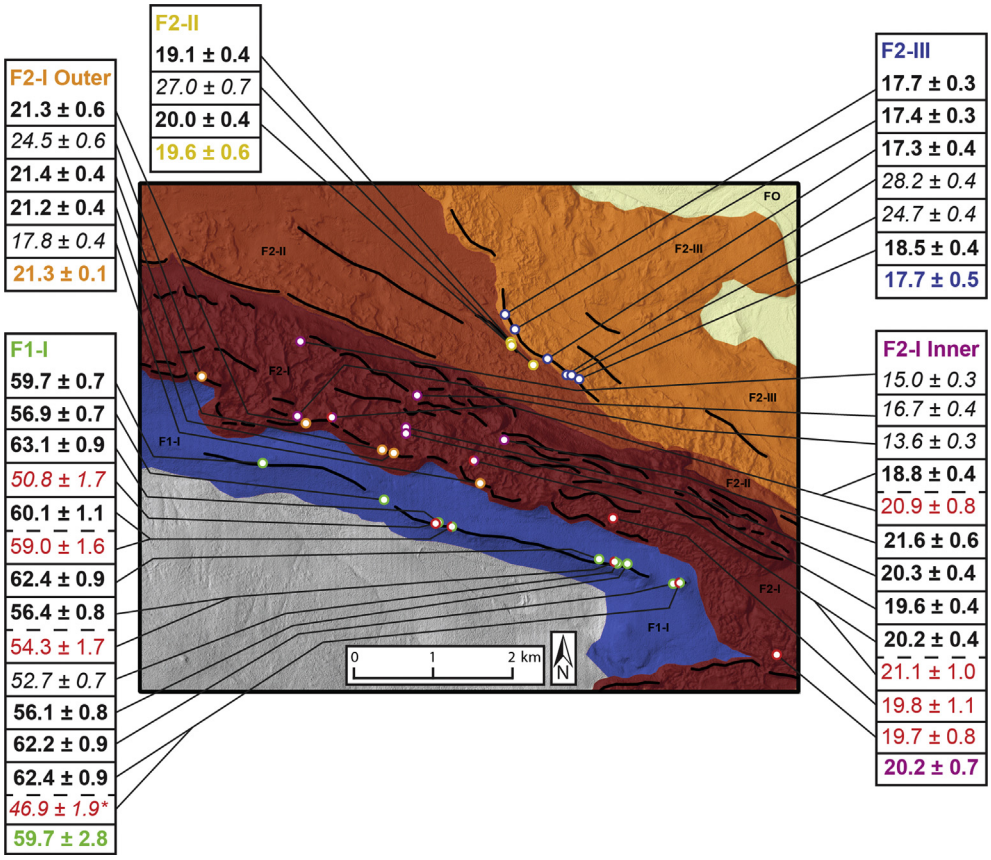

Fig. 4. Map of the field area showing each mapped moraine unit (see Fig. 2 for map unit legend) and ages from five morphostratigraphic units. Colored dots on map correspond to ages from each morphostratigraphic unit except for the dots in red, which represent pilot ages from Briner et al. (2005) that were not resampled. Dots that are half-red are from resampled boulders. Ages reported in black are from this study (italicized ages are outliers), and ages in red are pilot ages from Briner et al. (2005). Colored ages in each morphostratigraphic unit are average and 1 SD of bold ages in each group. *This sample was not reproduced within error; we have higher confidence in the resampled age and thus exclude the pilot age from our average calculations. (For interpretation of the references to color in this figure legend, the reader is referred to the Web version of this article.)

et al., 2009; Dortch et al., 2010; Pendleton et al., 2017). The marked occurrence of younger outliers from Farewell-II [MIS 2] moraines might thus be explained by the moraine's hummocky morphology. We also observe four instances of boulders with ages that seem anomalously old, likely influenced by isotopic inheritance. We find that all of these older ages can be statistically removed via Chauvenet's Criterion. We do not find any relationship between boulder dimensions and age. Despite these concerns, a majority of the ages in each group cluster well and are in stratigraphic order.

For the F1-I moraine, we prefer the interpretation that the average age of 59.7 ± 3.6 ka (n = 9; excluding two young outliers) represents the culmination of the early Wisconsinan [MIS 4] advance of the Swift River glacier. If post-depositional moraine degradation was significant, then one might favor the oldest ages as representing the timing of moraine deposition (in the absence of any obvious inheritance). However, we do not observe a young skew in the age distribution. Thus, we assign an age to the F1-I moraine using the average of our boulder ages. We did not date anything beyond the F1-I moraine, but we note moraine crests south of the F1-I moraine that are draped over a topographic high point (Fig. 2). While those moraines likely belong to a suite of pre-Wisconsinan moraines that exist in the region (Hamilton et al., 1986; Kaufman et al., 2011), it is possible that the early Wisconsinan terminal moraine lies somewhere beyond the one we dated. Therefore, the FI-1 moraine may be an early Wisconsinan recessional moraine.

We favor the interpretation that the average age of 21.3 ± 0.8 ka (n = 3; excluding one old and one young outlier from the outermost F2-I crest) represents the culmination of the maximum late Wisconsinan [MIS 2] glacier advance in the Swift River valley. Since a majority of the ages cluster well on the two recessional moraines that we dated, we have high confidence that the average ages for each moraine represent the timing of deposition at 19.6 ± 1.0 ka and 17.7 ± 0.8 ka, respectively. Assuming ice steadily retreated a distance of ca. 14 km between 21.3 ± 0.8 ka and 17.7 ± 0.8 ka, we calculate an average net retreat rate of 3.9 m a^{-1}.

Finally, we compare our ages to those from Briner et al. (2005). On the Farewell-I moraine, where weathering pits are common, three of our ages come from carefully re-sampled boulders [16SR1-01: this study, 60.1 ± 1.1 ka, Briner et al. (2005), 59.0 ± 1.6; 16SR1-08: this study, 56.4 ± 0.8, Briner et al. (2005), 54.3 ± 1.7 ka; 16SR1-11: this study, 62.4 ± 0.9 ka, Briner et al. (2005), 46.9 ± 1.9 ka], and two of the three ages are reproduced within error. We do not include the pilot age of 46.9 ± 1.9 ka in our age assignment of the F1-I moraine. On the F2-I inner discontinuous crests, two of our ages are also re-sampled and reproduced within error. The two remaining ages from the pilot study overlap with our ages; we include all four pilot ages in our age assignment of the inner F2-I moraines.

5.2. Wisconsinan glaciation in and out of Beringia

Moraines recording glacier advance during MIS 4 outside Beringia are uncommon. In most regions, moraines deposited

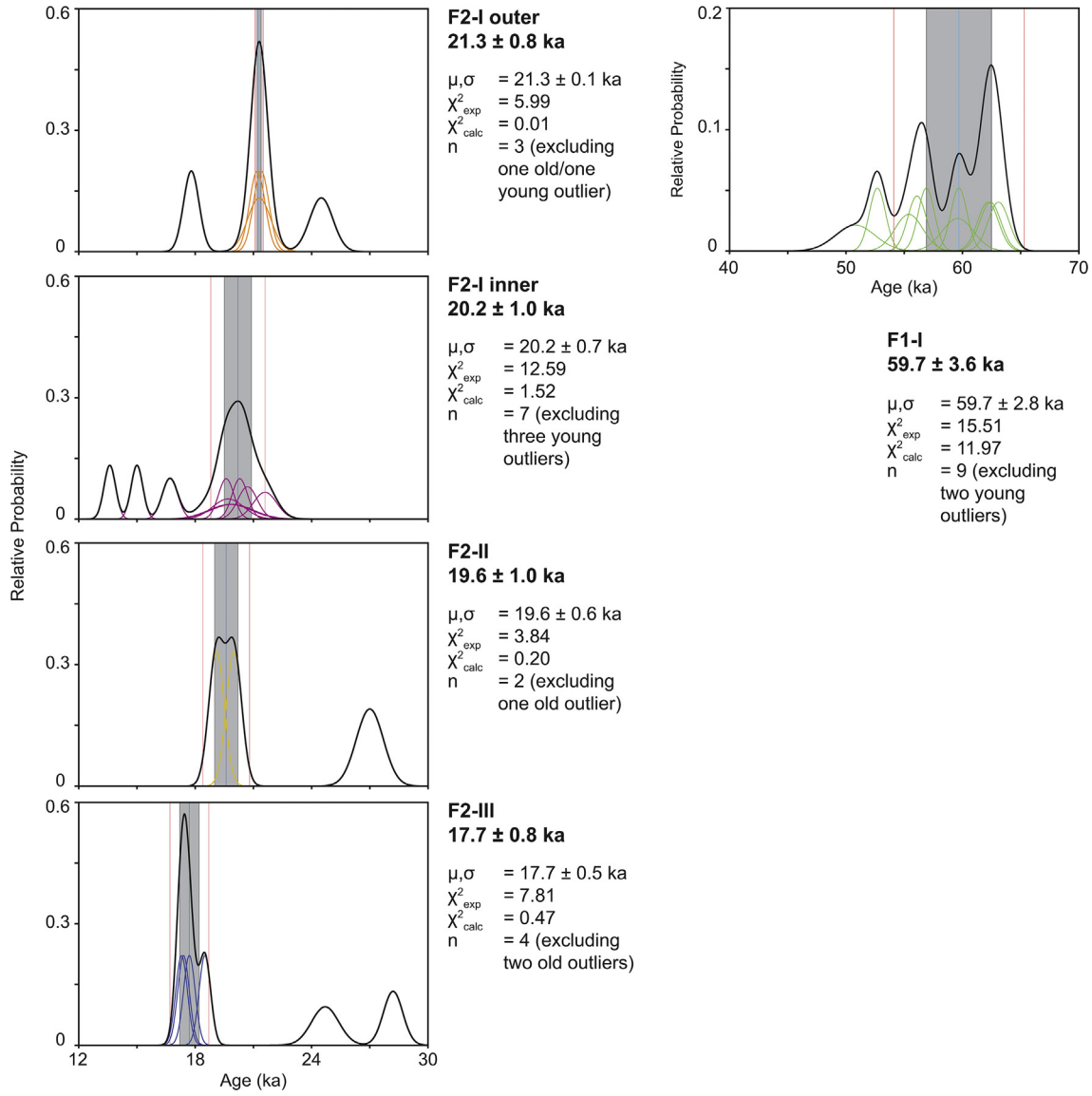

Fig. 5. Relative probability plots of ages from each morphostratigraphic unit. Colored lines represent age and reported 1 SD uncertainty, and black lines are summed probabilities. Colored lines in each morphostratigraphic unit correspond to colored dots from Fig. 4. Vertical lines in each morphostratigraphic unit represent the average (in blue), 1 SD within grey boxes, and 2 SD (red lines) excluding outliers. Average ages and 1 SD reported exclude outliers, and are calculated with (in bold) and without the Arctic Production rate uncertainty of 3.7% (Young et al., 2013). (For interpretation of the references to color in this figure legend, the reader is referred to the Web version of this article.)

during MIS 6 lie outboard of LGM moraines, and it is likely that LGM glaciers obliterated moraines deposited during MIS 4 (e.g., Ehlers et al., 2011). Multiple studies that find evidence for an ice advance between MIS 6 and MIS 2 report either few ages or largely scattered ages that are difficult to precisely compare with our record [e.g., High Atlas Mountains, Hughes et al. (2018); Southeastern Tibet, Owen et al. (2005); Tien Shan and Pamir, Zech et al. (2005); Abramowski et al. (2006), Koppes, et al. (2008); Zech (2012); Lifton et al. (2014b); Eastern Tien Shan, Chen et al. (2015); Pyrenees, Calvet et al. (2011); Rodríguez-Rodríguez et al. (2016), Japan; Sawagaki and Aoki (2011)]. Nonetheless, in the Southern Hemisphere, Schaefer et al. (2015) report ^{10}Be ages from South Island, NZ averaging 65.1 ± 2.8 ka (n = 36; total uncertainty is 1 SD with local production rate uncertainty of 2.5% propagated through; Putnam et al., 2010), and Peltier et al. (2016) report ^{10}Be ages from a moraine in Tierra del Fuego averaging 67.6 ± 3.9 ka (n = 6; total uncertainty is 1 SD with local production rate uncertainty of 2.9% propagated through; Kaplan et al., 2011).

Schaefer et al. (2015) note that multiple proxies (e.g., global CO_2, Southern Ocean de-stratification, eustatic sea level rise, ITCZ position, and NGRIP ice core $\delta^{18}O$) indicate that while the Southern Hemisphere began warming at the MIS 4/3 transition, the North Atlantic diverged into cold, stadial conditions (i.e., Heinrich Stadial 6 (HS-6); ca. 64–60 ka; Meese et al., 1997; Hemming, 2004). They interpret the moraine age of 65.1 ± 2.8 ka in the Southern Alps of New Zealand as deglaciation in response to Southern Hemisphere warming throughout HS-6. Whereas ages from the Southern Hemisphere reveal a glacial termination near the onset of HS-6, our ages from the Swift River valley and those from other sites in Beringia (e.g., Briner et al., 2001; Dortch et al., 2010) indicate a glacial culmination for the region at the end of HS-6 (Fig. 6). We suggest that Heinrich Stadial conditions extended beyond the North Atlantic into much of the high northern latitudes, thus explaining the ca. 5 kyr offset between our ages and those from the Southern Hemisphere.

^{10}Be and ^{14}C ages from alpine glaciers across Beringia suggest

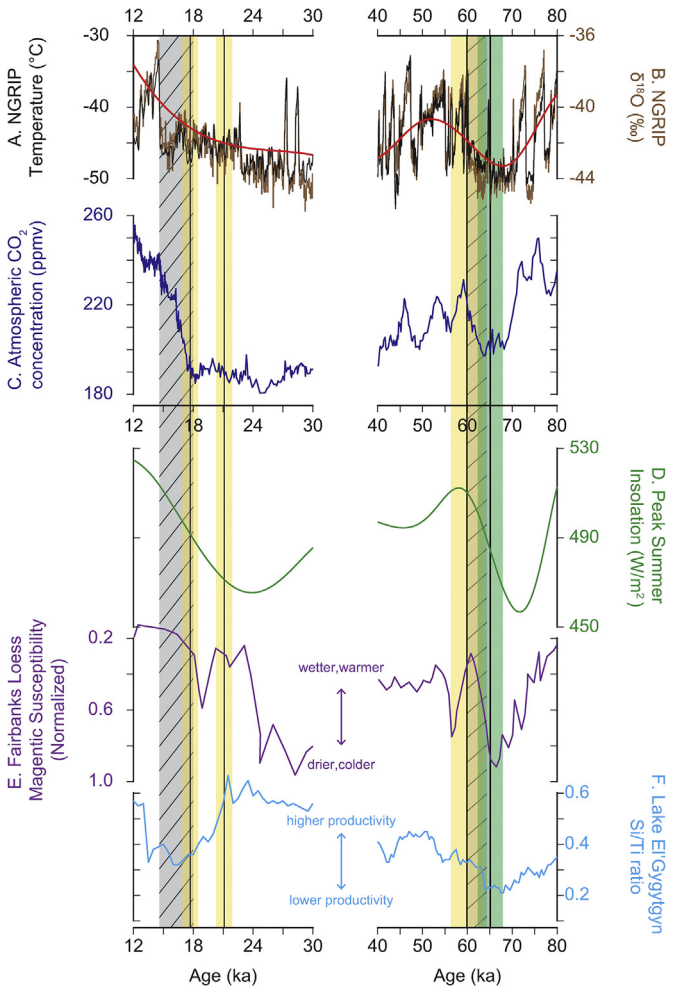

Fig. 6. Global and Arctic records spanning 30–12 ka and 80–40 ka. Included are average moraine ages (black bars) and 1 SD uncertainties (with production rate uncertainty propagated through; yellow bars) from the F1-I moraine (59.7 ± 3.6 ka) and the outer F2-I moraine (21.3 ± 0.8 ka) and F2-III moraine (17.7 ± 0.8 ka). HS-1 (ca. 18–14.6 ka) and HS-6 (ca. 64–60 ka) noted in grey hatched bars. MIS 4 ages from Schaefer et al. (2015) in light green. Global records in the top two panels, and local Beringia records in the bottom three panels. From top to bottom.: A) Surface air temperature record from the NGRIP ice core based on $\delta^{15}N$ measurements (Kindler et al., 2014). Absolute measurements plotted on black line; 10 kyr cubic spline of absolute measurements plotted in red. B) $\delta^{18}O$ measurements from the NGRIP ice core. C) Composite atmospheric CO2 concentration measurements from EPICA members Antarctic ice cores (Bereiter et al., 2015). D) Peak summer insolation (June 21) for 61.5°N, the approximate latitude of the Swift River valley (Laskar et al., 2004). E) Local normalized magnetic susceptibility record from outside of Fairbanks, AK (Begét, 1996). F) Si/Ti ratios from a lake sediment core collected in Lake El'Gygytgyn (Melles et al., 2012). (For interpretation of the references to color in this figure legend, the reader is referred to the Web version of this article.)

that the culmination of the late Wisconsinan advance may have occurred synchronously around ca. 21 ka (e.g., Briner et al., 2017), which is supported by our record. Furthermore, our record, along with the few records that precisely date recessional alpine glacier moraines in Beringia, indicate significant retreat between ca. 21 and 18 ka (ca. 25% in the case of alpine glaciers in the Revelation Mountains). While LGM termination in Beringia is consistent with compiled global records (Clark et al., 2012; Shakun et al., 2015), alpine glaciers in the region apparently experienced substantial retreat prior to rising CO_2 concentrations at ca. 18 ka (Fig. 6). We hypothesize that amplified high-latitude warming from rising insolation forced a greater magnitude of initial alpine glacier retreat in Beringia compared to glaciated regions in lower latitudes.

5.3. Paleoclimate history of Beringia

To date, there exists no well-dated, continuous paleoenvironmental reconstruction that spans MIS 4 in Beringia. However, two loess records, one from the Kurtak area of southern Siberia (Chlachula et al., 1997, 1998) and the other from near Fairbanks, Alaska (Fig. 6; Begét, 1996), span the early and late Wisconsinan phases. Geochronologic controls are limited, and hinge on tuning the records to the global deep-ocean oxygen isotope stack (Begét, 2001). If correctly dated, magnetic susceptibility values from both records during MIS 4 are comparable to magnetic susceptibility values during both MIS 6 and MIS 2. This implies glacial conditions during MIS 4, which is consistent with the moraine record in Beringia. Arctic ground squirrel middens recovered from Loess deposits in the Klondike further demonstrate that MIS 4 environmental conditions in the region were similar to MIS 2 (Zazula et al., 2011).

Despite the widespread occurrence of ice-free areas in Alaska during the Wisconsinan glaciation, lake sediment records that span the entire glacial cycle are rare. Those that exist are not well-dated, and continuous climatic reconstructions have not been attempted (e.g., Shackleton, 1982). Thus far, the only precisely dated, continuous lake record spanning multiple glaciations in Beringia comes from Lake El'Gygytgyn (e.g., Nowaczyk et al., 2002; Melles et al., 2007, 2012). Near-continuous ice cover likely resulted in anoxic bottom conditions in the lake over both MIS 4 and MIS 2, as evidenced by high TOC values. Magnetic susceptibility values for MIS 4 and MIS 2 dated sediments are comparable, suggestive of low productivity and cold temperatures. However, Si/Ti ratios reveal the lowest lake productivity – which potentially indicates lowest summer temperatures – occurred during MIS 4 (Fig. 6). Lastly, $\delta^{15}N$ measurements from the NGRIP ice core depict MIS 4 and MIS 2 temperature depressions occurring in phase with early and late Wisconsinan glacier advances in Beringia (Fig. 6; Kindler et al., 2014). We note a slightly larger temperature depression during MIS 4 compared to MIS 2 (Fig. 6).

Several paleoenvironmental reconstructions spanning through MIS 2 in Beringia indicate that summer conditions in the region were much drier and likely colder than present. For example, at Burial Lake, northwestern Brooks Range, a hiatus in sedimentation from 34.8 to 23.2 kyr BP marks a lake level lowstand and arid conditions (Abbott et al., 2010; Finkenbinder et al., 2015). In addition, Dorfman et al. (2015) presented a continuous record from MIS 3 through the Holocene from a second site in Burial Lake that depicts the highest S-Ratios (a proxy for dust flux into lake basins) from late MIS 3 through MIS 2 (37.2–19.4 cal kyr BP). Combined, Burial Lake records suggest that gusty and arid conditions likely prevailed in the region during late MIS 3 through MIS 2. Pollen reconstructions from the Tanana Upland suggest that herb taxa persisted during MIS 2 most likely because of arid conditions and depressed growing season temperatures (Finkenbinder et al., 2014; Schirrmeister et al., 2016). In the Klondike region of central Yukon, numerous ground squirrel middens and megafauna fossils have been collected in stratigraphic beds corresponding to MIS 2 (e.g. Froese et al., 2009). These remains further depict a "steppe-tundra hybrid" paleoenvironment in Beringia with colder than present growing seasons and less moisture (Zazula et al., 2007). Finally, a temperature reconstruction based on fossil chironomids collected in a lake core near the Bering Sea shows depressed early MIS 2 (prior to ca. 25 cal kyr BP) temperatures with a steady increase in temperature between ca. 23–17 cal kyr BP (Kurek et al., 2009).

Temperature reconstructions at 21 ka from pollen records using modern analogue techniques, on the other hand, suggest mean annual temperatures and mean coldest month temperatures comparable to today in the region (Bartlein et al., 2011). While

Finkenbinder et al. (2015) argue that their paleoenvironmental reconstructions reflect summer growing seasons, Bartlein et al. (2011) suggested that enhanced southerly advection in wintertime caused by the strong pressure gradient between the Aleutian Low and the high pressure system that developed over the Laurentide Ice Sheet (LIS) kept winter temperatures much warmer than present. Indeed, model simulations conducted with the Community Climate System Model Version 3 (CCSM3) demonstrate enhanced winter warming in Beringia during MIS 2 driven by southerly advection (Otto-Bliesner et al., 2006; Löfverström and Liakka, 2016). These discrepancies, and the potential effect of seasonality on mean annual temperatures in Beringia during MIS 2, are yet to be resolved.

5.4. On the relative extent of Wisconsinan glaciations in Beringia

We next investigate possible climate forcing of early [MIS 4] and late [MIS 2] Wisconsinan glacier advances. Causes for relatively restricted late Wisconsinan ice in Beringia remain uncertain. A long-standing hypothesis invokes the emergence of the Bering Land Bridge as a mechanism for limiting moisture transport to Beringia during the LGM, effectively hindering the advance of local glaciers (Brigham-Grette, 2001; Briner et al., 2005). Eustatic sea level was ca. 95 m and 120 m below present sea level during MIS 4 and MIS 2, respectively, and the Bering Land Bridge was exposed during both periods (Brigham-Grette, 2001; Ager, 2003; Siddall et al., 2003, Fig. 7). Because eustatic sea level was lower and slightly more of the Bering Land Bridge was exposed during MIS 2 than during MIS 4, it is possible that limited moisture transport hindered glacier advance more strongly during MIS 2. However, these relatively small differences in MIS 4 versus MIS 2 eustatic sea level do not equate to significant differences in the distance to moisture source during the two time periods (Fig. 7).

New lines of evidence reveal other possible forcing mechanisms driving glacier advances in Beringia. Emerging evidence from NGRIP and Lake El'Gygytgyn suggest that temperatures in Beringia, and possibly the broader high northern latitudes, may have been colder during MIS 4 than during MIS 2 (Melles et al., 2012; Kindler et al., 2014, Fig. 6). Thus, it is possible that colder temperature forced Beringian glaciers during MIS 4 to be more expansive than during MIS 2. Furthermore, Löfverström and Liakka (2016) found that modeled surface temperature in Beringia during the LGM was strongly modulated by diabatic warming and changes in planetary albedo in the summer, and enhanced southerly advection forced by the LIS (particularly in the winter as previously discussed). Because the insolation minimum during MIS 4 was lower than during MIS 2 (Fig. 6), surface temperature in Beringia may have been colder due to a reduction in diabatic warming. We note that in a region with sufficient mean annual precipitation (>250 mm/yr), alpine glaciers are more sensitive to temperature variablility than precipitation

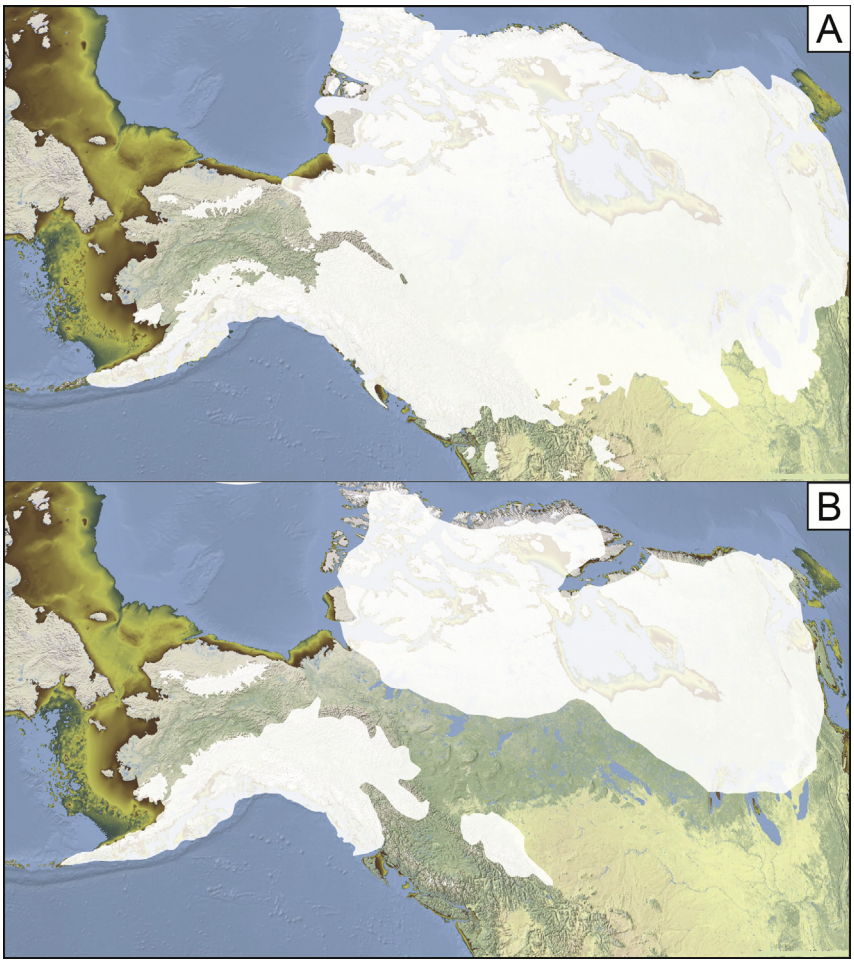

Fig. 7. Reconstruction of the extent of the Bering Land Bridge A) during MIS 2 when eustatic sea level was 120 m below present and B) during MIS 4 when eustatic sea level was 95 m below present [based on eustatic sea level curves from Siddall et al. (2003)]. Extent of the LIS during MIS 2 from Dyke (2004) and modeled maximum ice sheet extent during MIS 4 re-drawn from Kleman et al. (2013). Ice extents in Alaska during both phases from Kaufman et al. (2011). We acknowledge that MIS 4 extent for the CIS is not in full agreement with field data in the Yukon (e.g. Duk-Rodkin, 1999; Ward et al., 2007, 2008; Turner et al., 2013) nor in British Columbia (e.g. Mathewes et al., 2015).

variability (Rupper and Roe, 2008).

In addition, Löfverström and Liakka (2016) also suggested a reduction in moisture transport to Beringia during MIS 2 in response to low sea surface temperatures in the northern Pacific Ocean. While the air masses advected into Beringia may have been warm, they were also likely dry, indicating that arid conditions may have further contributed to limited late Wisconsinan glacier advance.

Additionally, we compare glacier extent in Beringia to the extent of the LIS over the Wisconsinan glaciation. If atmospheric reorganization forced by LIS size exerts a primary control on the climate of Beringia as Löfverström and Liakka (2016) suggest, then it would follow that the region was colder and wetter during MIS 4 than MIS 2. Model simulations and geomorphic evidence (Kleman et al., 2010, 2013, Fig. 7) suggest the LIS did not extend as far west during MIS 4, and thus potentially had a weaker influence on atmospheric circulation over the Pacific Ocean and Beringia. We hypothesize that varying sizes of the LIS between MIS 4 and MIS 2 might explain why it was colder and wetter in Beringia during MIS 4 than during MIS 2, and therefore why glaciers were larger.

6. Conclusions

We provide a new moraine chronology of early and late Wisconsinan glaciation in the Revelation Mountains, Alaska. Our chronology shows that the early Wisconsinan phase culminated at 59.7 ± 3.6 ka (average, $n = 9$), and the late Wisconsinan phase culminated at 21.3 ± 0.8 ka (average, $n = 3$). The chronology also reveals substantial ice retreat from the maximum late Wisconsinan extent from 21.3 ± 0.8 ka to 17.7 ± 0.8 ka.

We find that the early Wisconsinan phase did not culminate until the close of HS-6, despite a preceding interval of sustained insolation and CO_2 concentration increase. We suggest that the early Wisconsinan advance terminated in response to far-field abrupt warming in the North Atlantic region at the close of HS-6. Conversely, we found that during MIS 2, glacier retreat began ca. 21 ka and the glacier had retreated to 25% of its full late Wisconsinan length prior to the increase in atmospheric CO_2 at ca. 18 ka. We suggest that increasing insolation prompted regional warming, perhaps amplified in high northern latitudes, which initiated glacier retreat in Beringia during MIS 2.

Regarding the preservation of MIS 4 moraines in Beringia, we suggest two possible mechanisms. First, the early Wisconsinan advance followed inferred coldest conditions observed in both the Lake El'Gygytgyn record and the NGRIP record at ca. 70–60 ka. In addition, the early Wisconsinan phase occurred when peak summer insolation was lower than during MIS 2. We suggest that summer temperature may have been colder in Beringia during MIS 4 than MIS 2, resulting in more extensive glacier advance.

Second, we observe an inverse pattern of Wisconsinan glaciation between Beringian glaciers and the LIS during stadial conditions. Beringian glaciers are large when the LIS is reduced in size, but relatively restricted when the LIS is at its maximum phase. Model simulations show that when enlarged, the LIS re-organizes atmospheric circulation patterns over the Pacific Ocean, driving storm tracks southward and advecting warm air into Beringia, particularly in the wintertime when the Aleutian Low is strongest. Moreover, during the LGM, low sea surface temperatures in the north Pacific Ocean forced the air advected into Beringia to be relatively dry. We hypothesize that due to variable sizes of the LIS during early and late Wisconsinan phases, climate in Beringia was more strongly impacted by the LIS during MIS 2 than during MIS 4. Future work will help elucidate the role of forcing mechanisms discussed here (e.g., CO_2, Heinrich events, the LIS and insolation) in controlling the advance and retreat patterns of Wisconsinan glaciation.

Acknowledgements

We thank A. Schweinsberg and C. Sbarra at the University at Buffalo for assistance with the laboratory work, and the Center for Mass Spectrometry at Lawrence Livermore National Laboratory for ^{10}Be measurements. This research was funded in part by the John T. Dillon Alaska Research Award through the Geological Society of America, the Mark Diamond Research Grant through the University at Buffalo's Graduate Student Association, and the Duane Champion Summer Travel Fund through the University at Buffalo's Geology Department. We would also like to thank Regal Air Floatplane Charter Company for swift and safe travels in the field. We thank Dr. Brent Ward and one other anonymous reviewer for their thorough and thoughtful comments which greatly improved the quality of this manuscript. This is LDEO publication #8245.

Appendix A. Supplementary data

Supplementary data related to this article can be found at https://doi.org/10.1016/j.quascirev.2018.08.009.

References

Abbott, M.B., Edwards, M.E., Finney, B.P., 2010. A 40,000-yr record of environmental change from Burial Lake in Northwest Alaska. Quat. Res. 74 (1), 156–165.
Abramowski, U., Bergau, A., Seebach, D., Zech, R., Glaser, B., Sosin, P., Kubik, P.W., Zech, W., 2006. Pleistocene glaciations of Central Asia: results from 10Be surface exposure ages of erratic boulders from the Pamir (Tajikistan), and the Alay–Turkestan range (Kyrgyzstan). Quat. Sci. Rev. 25 (9), 1080–1096.
Ager, T.A., 2003. Late Quaternary vegetation and climate history of the central Bering land bridge from St. Michael Island, western Alaska. Quat. Res. 60 (1), 19–32.
Balascio, N.L., Kaufman, D.S., Briner, J.P., Manley, W.F., 2005. Late Pleistocene glacial geology of the Okpilak-Kongakut rivers region, northeastern Brooks Range, Alaska. Arctic Antarct. Alpine Res. 37 (4), 416–424.
Balco, G., Briner, J., Finkel, R.C., Rayburn, J.A., Ridge, J.C., Schaefer, J.M., 2009. Regional beryllium-10 production rate calibration for late-glacial northeastern North America. Quat. Geochronol. 4 (2), 93–107.
Bartlein, P., Harrison, S., Brewer, S., Connor, S., Davis, B., Gajewski, K., Guiot, J., Harrison-Prentice, T., Henderson, A., Peyron, O., 2011. Pollen-based continental climate reconstructions at 6 and 21 ka: a global synthesis. Clim. Dynam. 37 (3–4), 775–802.
Begét, J.E., 1996. Tephrochronology and paleoclimatology of the last interglacial-glacial cycle recorded in Alaskan loess deposits. Quat. Int. 34, 121–126.
Begét, J.E., 2001. Continuous Late Quaternary proxy climate records from loess in Beringia. Quat. Sci. Rev. 20 (1), 499–507.
Bereiter, B., Eggleston, S., Schmitt, J., Nehrbass-Ahles, C., Stocker, T.F., Fischer, H., Kipfstuhl, S., Chappellaz, J., 2015. Revision of the EPICA Dome C CO2 record from 800 to 600 kyr before present. Geophys. Res. Lett. 42 (2), 542–549.
Borchers, B., Marrero, S., Balco, G., Caffee, M., Goehring, B., Lifton, N., Nishiizumi, K., Phillips, F., Schaefer, J., Stone, J., 2016. Geological calibration of spallation production rates in the CRONUS-Earth project. Quat. Geochronol. 31, 188–198.
Brigham-Grette, J., 2001. New perspectives on Beringian Quaternary paleogeography, stratigraphy, and glacial history. Quat. Sci. Rev. 20 (1), 15–24.
Brigham-Grette, J., Gualtieri, L.M., Glushkova, O.Y., Hamilton, T.D., Mostoller, D., Kotov, A., 2003. Chlorine-36 and 14C chronology support a limited last glacial maximum across central chukotka, northeastern Siberia, and no Beringian ice sheet. Quat. Res. 59 (3), 386–398.
Briner, J.P., Swanson, T.W., Caffee, M., 2001. Late Pleistocene cosmogenic 36 Cl glacial chronology of the southwestern Ahklun Mountains, Alaska. Quat. Res. 56 (2), 148–154.
Briner, J.P., Kaufman, D.S., Manley, W.F., Finkel, R.C., Caffee, M.W., 2005. Cosmogenic exposure dating of late Pleistocene moraine stabilization in Alaska. Geol. Soc. Am. Bull. 117 (7–8), 1108–1120.
Briner, J.P., Tulenko, J., Young, N., Baichtal, J., Lesnek, A., 2017. The last deglaciation of Alaska. Cuadernos Invest. Geogr. 43 (2), 429–448.
Calvet, M., Delmas, M., Gunnell, Y., Braucher, R., Bourlès, D., 2011. Recent Advances in Research on Quaternary Glaciations in the Pyrenees, Developments in Quaternary Sciences, vol. 15. Elsevier, pp. 127–139.
Chen, Y., Li, Y., Wang, Y., Zhang, M., Cui, Z., Yi, C., Liu, G., 2015. Late Quaternary glacial history of the Karlik Range, easternmost Tian Shan, derived from 10Be surface exposure and optically stimulated luminescence datings. Quat. Sci. Rev. 115, 17–27.
Child, J., 1995. A Late Quaternary Lacustrine Record of Environmental Change in the Wonder Lake Area, Denali National Park and Preserve, Alaska. University of Massachusetts at Amherst.
Chlachula, J., Evans, M., Rutter, N., 1998. A magnetic investigation of a Late Quaternary loess/palaeosol record in Siberia. Geophys. J. Int. 132 (1), 128–132.

Chlachula, J., Rutter, N., Evans, M., 1997. A late Quaternary loess–paleosol record at Kurtak, southern Siberia. Can. J. Earth Sci. 34 (5), 679–686.
Clark, P.U., Dyke, A.S., Shakun, J.D., Carlson, A.E., Clark, J., Wohlfarth, B., Mitrovica, J.X., Hostetler, S.W., McCabe, A.M., 2009. The last glacial maximum. Science 325 (5941), 710–714.
Clark, P.U., Shakun, J.D., Baker, P.A., Bartlein, P.J., Brewer, S., Brook, E., Carlson, A.E., Cheng, H., Kaufman, D.S., Liu, Z., Marchitto, T.M., Mix, A.C., Morrill, C., Otto-Bliesner, B.L., Pahnke, K., Russell, J.M., Whitlock, C., Adkins, J.F., Blois, J.L., Clark, J., Colman, S.M., Curry, W.B., Flower, B.P., He, F., Johnson, T.C., Lynch-Stieglitz, J., Markgraf, V., McManus, J., Mitrovica, J.X., Moreno, P.I., Williams, J.W., 2012. Global climate evolution during the last deglaciation. Proc. Natl. Acad. Sci. Unit. States Am. 109 (19), E1134–E1142.
Corbett, L.B., Bierman, P.R., Rood, D.H., 2016. An approach for optimizing in situ cosmogenic 10 Be sample preparation. Quat. Geochronol. 33, 24–34.
Dorfman, J., Stoner, J., Finkenbinder, M., Abbott, M., Xuan, C., St-Onge, G., 2015. A 37,000-year environmental magnetic record of aeolian dust deposition from Burial Lake, Arctic Alaska. Quat. Sci. Rev. 128, 81–97.
Dortch, J.M., Owen, L.A., Caffee, M.W., Li, D., Lowell, T.V., 2010. Beryllium-10 surface exposure dating of glacial successions in the Central Alaska Range. J. Quat. Sci. 25 (8), 1259–1269.
Duk-Rodkin, A., 1999. Glacial Limits Map of Yukon Territory: Geological Survey of Canada, Open File 3694, Scale 1:1,000,000.
Dyke, A.S., 2004. An outline of North American deglaciation with emphasis on central and northern Canada. Dev. Quat. Sci. 2, 373–424.
Ehlers, J., Gibbard, P.L., Hughes, P.D., 2011. Quaternary Glaciations-extent and Chronology: a Closer Look. Elsevier.
Fernald, A.T., 1953. Alaska Range in Upper Kuskokwim Region, Alaska: Multiple Glaciations in Alaska. USGS, p. 6.
Finkenbinder, M., Abbott, M., Finney, B., Stoner, J., Dorfman, J., 2015. A multi-proxy reconstruction of environmental change spanning the last 37,000 years from Burial Lake, Arctic Alaska. Quat. Sci. Rev. 126, 227–241.
Finkenbinder, M.S., Abbott, M.B., Edwards, M.E., Langdon, C.T., Steinman, B.A., Finney, B.P., 2014. A 31,000 year record of paleoenvironmental and lake-level change from Harding Lake, Alaska, USA. Quat. Sci. Rev. 87, 98–113.
Froese, D.G., Zazula, G.D., Westgate, J.A., Preece, S.J., Sanborn, P.T., Reyes, A.V., Pearce, N.J., 2009. The Klondike goldfields and Pleistocene environments of Beringia. GSA Today (Geol. Soc. Am.) 19 (8), 4–10.
Hamilton, T.D., 1994. Late cenozoic glaciation of Alaska. In: Plafker, G., Berg, H.C. (Eds.), The Geology of Alaska, G-1. Geological Society of America, pp. 813–844.
Hamilton, T.D., Reed, K.M., Thorson, R.M., 1986. Glaciation in Alaska: the Geologic Record. Alaska Geological Society.
Hemming, S.R., 2004. Heinrich events: massive late Pleistocene detritus layers of the North Atlantic and their global climate imprint. Rev. Geophys. 42 (1).
Hughes, P.D., Fink, D., Rodés, Á., Fenton, C.R., Fujioka, T., 2018. Timing of Pleistocene glaciations in the high Atlas, Morocco: new 10Be and 36Cl exposure ages. Quat. Sci. Rev. 180, 193–213.
Hughes, A.L., Gyllencreutz, R., Lohne, Ø.S., Mangerud, J., Svendsen, J.I., 2016. The last Eurasian ice sheets–a chronological database and time-slice reconstruction, DATED-1. Boreas 45 (1), 1–45.
Kaplan, M.R., Strelin, J.A., Schaefer, J.M., Denton, G.H., Finkel, R.C., Schwartz, R., Putnam, A.E., Vandergoes, M.J., Goehring, B.M., Travis, S.G., 2011. In-situ cosmogenic 10Be production rate at Lago Argentino, Patagonia: implications for late-glacial climate chronology. Earth Planet Sci. Lett. 309 (1–2), 21–32.
Kaufman, D.S., Hu, F.S., Briner, J.P., Werner, A., Finney, B.P., Gregory-Eaves, I., 2003. Ã 33,000 year record of environmental change from Arolik Lake, Ahklun mountains, Alaska, USA. J. Paleolimnol. 30 (4), 343–361.
Kaufman, D.S., Jensen, B.J.L., Reyes, A.V., Schiff, C.J., Froese, D.G., Pearce, N.J.G., 2012. Late quaternary tephrostratigraphy, Ahklun mountains, SW Alaska. J. Quat. Sci. 27 (4), 344–359.
Kaufman, D.S., Manley, W.F., 2004. Pleistocene maximum and Late Wisconsinan glacier extents across Alaska, USA. Dev. Quat. Sci. 2, 9–27.
Kaufman, D.S., Young, N.E., Briner, J.P., Manley, W.F., 2011. Alaska paleo-glacier Atlas (version 2). In: Ehlers, J., Gibbard, P.L., Hughes, P. (Eds.), Quaternary Glaciations - Extent and Chronology, vol. 15. Developments in Quaternary Science, Amsterdam, Netherlands.
Kindler, P., Guillevic, M., Baumgartner, M., Schwander, J., Landais, A., Leuenberger, M., 2014. Temperature reconstruction from 10 to 120 kyr b2k from the NGRIP ice core. Clim. Past 10 (2), 887–902.
Kleman, J., Fastook, J., Ebert, K., Nilsson, J., Caballero, R., 2013. Pre-LGM Northern Hemisphere ice sheet topography. Clim. Past 9 (5), 2365.
Kleman, J., Jansson, K., De Angelis, H., Stroeven, A.P., Hättestrand, C., Alm, G., Glasser, N., 2010. North American Ice Sheet build-up during the last glacial cycle, 115–21kyr. Quat. Sci. Rev. 29 (17), 2036–2051.
Kline, J.T., Bundtzen, T.K., 1986. Two glacial records from west-central Alaska. In: Hamilton, T.D., Reed, K.M., Thorson, R.M. (Eds.), Glaciation in Alaska: the Geologic Record. Alaska Geological Society, pp. 123–150.
Kohl, C., Nishiizumi, K., 1992. Chemical isolation of quartz for measurement of in-situ-produced cosmogenic nuclides. Geochem. Cosmochim. Acta 56 (9), 3583–3587.
Koppes, M., Gillespie, A.R., Burke, R.M., Thompson, S.C., Stone, J., 2008. Late quaternary glaciation in the kyrgyz tien Shan. Quat. Sci. Rev. 27 (7), 846–866.
Kurek, J., Cwynar, L.C., Ager, T.A., Abbott, M.B., Edwards, M.E., 2009. Late Quaternary paleoclimate of western Alaska inferred from fossil chironomids and its relation to vegetation histories. Quat. Sci. Rev. 28 (9), 799–811.
Lal, D., 1991. Cosmic ray labeling of erosion surfaces: in situ nuclide production rates and erosion models. Earth Planet Sci. Lett. 104 (2–4), 424–439.
Lanphere, M.A., Reed, B.L., 1985. The McKinley sequence of granitic rocks: a key element in the accretionary history of southern Alaska. J. Geophys. Res.: Solid Earth 90 (B13), 11413–11430.
Laskar, J., Robutel, P., Joutel, F., Gastineau, M., Correia, A., Levrard, B., 2004. A long-term numerical solution for the insolation quantities of the Earth. Astron. Astrophys. 428 (1), 261–285.
Lifton, N., Sato, T., Dunai, T.J., 2014a. Scaling in situ cosmogenic nuclide production rates using analytical approximations to atmospheric cosmic-ray fluxes. Earth Planet Sci. Lett. 386, 149–160.
Lifton, N., Beel, C., Hättestrand, C., Kassab, C., Rogozhina, I., Heermance, R., Oskin, M., Burbank, D., Blomdin, R., Gribenski, N., Caffee, M., Goehring, B.M., Heyman, J., Ivanov, M., Li, Y., Li, Y., Petrakov, D., Usubaliev, R., Codilean, A.T., Chen, Y., Harbor, J., Stroeven, A.P., 2014b. Constraints on the late Quaternary glacial history of the Inylchek and Sary-Dzaz valleys from in situ cosmogenic 10Be and 26Al, eastern Kyrgyz Tian Shan. Quat. Sci. Rev. 101, 77–90.
Löfverström, M., Liakka, J., 2016. On the limited ice intrusion in Alaska at the LGM. Geophys. Res. Lett. 43 (20).
Manley, W.F., Kaufman, D.S., Briner, J.P., 2001. Pleistocene glacial history of the southern Ahklun Mountains, southwestern Alaska: soil-development, morphometric, and radiocarbon constraints. Quat. Sci. Rev. 20 (1), 353–370.
Margold, M., Stroeven, A.P., Clague, J.J., Heyman, J., 2014. Timing of terminal Pleistocene deglaciation at high elevations in southern and central British Columbia constrained by 10Be exposure dating. Quat. Sci. Rev. 99, 193–202.
Mathewes, R.W., Lian, O.B., Clague, J.J., Huntley, M.J., 2015. Early wisconsinan (MIS 4) glaciation on Haida gwaii, british Columbia, and implications for biological refugia. Can. J. Earth Sci. 52 (11), 939–951.
Matmon, A., Briner, J., Carver, G., Bierman, P., Finkel, R., 2010. Moraine chronosequence of the donnelly Dome region, Alaska. Quat. Res. 74 (1), 63–72.
Meese, D., Gow, A., Alley, R., Zielinski, G., Grootes, P., Ram, M., Taylor, K., Mayewski, P.A., Bolzan, J., 1997. The Greenland Ice Sheet Project 2 depth-age scale: methods and results. J. Geophys. Res. Oceans 102 (C12), 26411–26423.
Melles, M., Brigham-Grette, J., Glushkova, O.Y., Minyuk, P.S., Nowaczyk, N.R., Hubberten, H.-W., 2007. Sedimentary geochemistry of core PG1351 from Lake El'gygytgyn—a sensitive record of climate variability in the East Siberian Arctic during the past three glacial–interglacial cycles. J. Paleolimnol. 37 (1), 89–104.
Melles, M., Brigham-Grette, J., Minyuk, P.S., Nowaczyk, N.R., Wennrich, V., DeConto, R.M., Anderson, P.M., Andreev, A.A., Coletti, A., Cook, T.L., 2012. 2.8 million years of Arctic climate change from Lake El'gygytgyn, NE Russia. Science 337 (6092), 315–320.
Miller, G.H., Alley, R.B., Brigham-Grette, J., Fitzpatrick, J.J., Polyak, L., Serreze, M.C., White, J.W., 2010. Arctic amplification: can the past constrain the future? Quat. Sci. Rev. 29 (15), 1779–1790.
Nishiizumi, K., Imamura, M., Caffee, M.W., Southon, J.R., Finkel, R.C., McAninch, J., 2007. Absolute calibration of 10 Be AMS standards. Nucl. Instrum. Methods Phys. Res. Sect. B Beam Interact. Mater. Atoms 258 (2), 403–413.
Nowaczyk, N., Minyuk, P., Melles, M., Brigham-Grette, J., Glushkova, O., Nolan, M., Lozhkin, A., Stetsenko, T., M. Andersen, P., Forman, S., 2002. Magnetostratigraphic results from impact crater Lake El'gygytgyn, northeastern Siberia: a 300 kyr long high-resolution terrestrial palaeoclimatic record from the Arctic. Geophys. J. Int. 150 (1), 109–126.
Otto-Bliesner, B.L., Brady, E.C., Clauzet, G., Tomas, R., Levis, S., Kothavala, Z., 2006. Last glacial maximum and Holocene climate in CCSM3. J. Clim. 19 (11), 2526–2544.
Owen, L.A., Finkel, R.C., Barnard, P.L., Haizhou, M., Asahi, K., Caffee, M.W., Derbyshire, E., 2005. Climatic and topographic controls on the style and timing of Late Quaternary glaciation throughout Tibet and the Himalaya defined by 10Be cosmogenic radionuclide surface exposure dating. Quat. Sci. Rev. 24 (12), 1391–1411.
Peltier, C., Kaplan, M., Schaefer, J., Soteres, R., Sagredo, E., Aravena, J., December 12-16 2016. A glacial chronology of the strait of magellan. In: Proceedings AGU Fall Meeting Abstracts.
Pendleton, S.L., Briner, J.P., Kaufman, D.S., Zimmerman, S.R., 2017. Using cosmogenic 10Be exposure dating and lichenometry to constrain Holocene glaciation in the central Brooks Range, Alaska. Arctic Antarct. Alpine Res. 49 (1), 115–132.
Pendleton, S.L., Ceperley, E.G., Briner, J.P., Kaufman, D.S., Zimmerman, S., 2015. Rapid and early deglaciation in the central Brooks range, arctic Alaska. Geology 43 (5), 419–422.
Pierce, K.L., 2003. Pleistocene Glaciations of the Rocky Mountains, Developments in Quaternary Sciences, vol. 1. Elsevier, pp. 63–76.
Porter, S.C., Pierce, K.L., Hamilton, T.D., 1983. Late Wisconsin mountain glaciation in the western United States. In: Wright, H.E., Porter, S.C. (Eds.), Late-quaternary Environments of the United States, vol. 1. University of Minnesota Press, Minnesota, pp. 71–111.
Putkonen, J., Connolly, J., Orloff, T., 2008. Landscape evolution degrades the geologic signature of past glaciations. Geomorphology 97 (1), 208–217.
Putkonen, J., Swanson, T., 2003. Accuracy of cosmogenic ages for moraines. Quat. Res. 59 (2), 255–261.
Putnam, A., Schaefer, J., Barrell, D., Vandergoes, M., Denton, G., Kaplan, M., Finkel, R., Schwartz, R., Goehring, B., Kelley, S., 2010. In situ cosmogenic 10Be production-rate calibration from the Southern Alps, New Zealand. Quat. Geochronol. 5 (4), 392–409.
Rodríguez-Rodríguez, L., Jiménez-Sánchez, M., Domínguez-Cuesta, M.J., Rinterknecht, V., Pallàs, R., Bourlès, D., 2016. Chronology of glaciations in the cantabrian mountains (NW iberia) during the last glacial cycle based on in situ-

produced 10Be. Quat. Sci. Rev. 138, 31–48.
Rupper, S., Roe, G., 2008. Glacier changes and regional climate: a mass and energy balance approach. J. Clim. 21 (20), 5384–5401.
Sawagaki, T., Aoki, T., 2011. Late Quaternary Glaciations in Japan, Developments in Quaternary Sciences, vol. 15. Elsevier, pp. 1013–1021.
Schaefer, J.M., Denton, G.H., Barrell, D.J., Ivy-Ochs, S., Kubik, P.W., Andersen, B.G., Phillips, F.M., Lowell, T.V., Schlüchter, C., 2006. Near-synchronous interhemispheric termination of the last glacial maximum in mid-latitudes. Science 312 (5779), 1510–1513.
Schaefer, J.M., Putnam, A.E., Denton, G.H., Kaplan, M.R., Birkel, S., Doughty, A.M., Kelley, S., Barrell, D.J.A., Finkel, R.C., Winckler, G., Anderson, R.F., Ninneman, U.S., Barker, S., Schwartz, R., Andersen, B.G., Schluechter, C., 2015. The southern glacial maximum 65,000 years ago and its unfinished termination. Quat. Sci. Rev. 114, 52–60.
Schirrmeister, L., Meyer, H., Andreev, A., Wetterich, S., Kienast, F., Bobrov, A., Fuchs, M., Sierralta, M., Herzschuh, U., 2016. Late quaternary paleoenvironmental records from the chatanika River Valley near Fairbanks (Alaska). Quat. Sci. Rev. 147, 259–278.
Shackleton, J., 1982. Environmental Histories from Whitefish and Imuruk Lakes, Seward Peninsula, Alaska. Institute of Polar Studies, The Ohio State University. Report No. 76.
Shakun, J.D., Clark, P.U., He, F., Marcott, S.A., Mix, A.C., Liu, Z., Otto-Bliesner, B., Schmittner, A., Bard, E., 2012. Global warming preceded by increasing carbon dioxide concentrations during the last deglaciation. Nature 484 (7392), 49–54.
Shakun, J.D., Clark, P.U., He, F., Lifton, N.A., Liu, Z., Otto-Bliesner, B.L., 2015. Regional and global forcing of glacier retreat during the last deglaciation. Nat. Commun. 6, 8059.
Sheinkman, V.S., 2011. Glaciation in the High Mountains of Siberia, Developments in Quaternary Sciences, vol. 15. Elsevier, pp. 883–907.
Siddall, M., Rohling, E.J., Almogi-Labin, A., Hemleben, C., Meischner, D., Schmelzer, I., Smeed, D.A., 2003. Sea-level fluctuations during the last glacial cycle. Nature 423, 853.
Stone, J.O., 2000. Air pressure and cosmogenic isotope production. J. Geophys. Res.: Solid Earth 105 (B10), 23753–23759.
Stroeven, A.P., Heyman, J., Fabel, D., Björck, S., Caffee, M.W., Fredin, O., Harbor, J.M., 2015. A new Scandinavian reference 10 Be production rate. Quat. Geochronol. 29, 104–115.
Ten Brink, N.W., Waythomas, C.F., 1985. Late Wisconsin Glacial Chronology of the North-Central Alaska Range–a Regional Synthesis and its Implications for Early Human Settlements.
Turner, D.G., Ward, B.C., Bond, J.D., Jensen, B.J.L., Froese, D.G., Telka, A.M., Zazula, G.D., Bigelow, N.H., 2013. Middle to Late Pleistocene ice extents, tephrochronology and paleoenvironments of the White River area, southwest Yukon. Quat. Sci. Rev. 75, 59–77.
Wahrhaftig, C., Black, R., 1958. Quaternary Geology of the Nenana River valley and Adjacent Parts of the Alaska Range; Engineering Geology along Part of the Alaska Railroad, 2330-7102.
Ward, B.C., Bond, J.D., Gosse, J.C., 2007. Evidence for a 55–50 ka (early Wisconsin) glaciation of the Cordilleran ice sheet, Yukon Territory, Canada. Quat. Res. 68 (1), 141–150.
Ward, B.C., Bond, J.D., Froese, D., Jensen, B., 2008. Old Crow tephra (140±10 ka) constrains penultimate Reid glaciation in central Yukon Territory. Quat. Sci. Rev. 27 (19–20), 1909–1915.
Werner, A., Wright, K., Child, J., 1993. Bluff stratigraphy along the McKinley River; a record of late Wisconsin climatic change. In: Proceedings Geological Society of America Abstracts with Programs, vol. 25. A224.
Young, N.E., Briner, J.P., Kaufman, D.S., 2009. Late Pleistocene and Holocene glaciation of the fish lake valley, northeastern Alaska range, Alaska. J. Quat. Sci. 24 (7), 677–689.
Young, N.E., Schaefer, J.M., Briner, J.P., Goehring, B.M., 2013. A 10Be production-rate calibration for the Arctic. J. Quat. Sci. 28 (5), 515–526.
Zazula, G.D., Froese, D.G., Elias, S.A., Kuzmina, S., Mathewes, R.W., 2007. Arctic ground squirrels of the mammoth-steppe: paleoecology of Late Pleistocene middens (~ 24 000–29 450 14C yr BP), Yukon Territory, Canada. Quat. Sci. Rev. 26 (7–8), 979–1003.
Zazula, G.D., Froese, D.G., Elias, S.A., Kuzmina, S., Mathewes, R.W., 2011. Early Wisconsinan (MIS 4) Arctic ground squirrel middens and a squirrel-eye-view of the mammoth-steppe. Quat. Sci. Rev. 30 (17), 2220–2237.
Zech, R., 2012. A late Pleistocene glacial chronology from the Kitschi-Kurumdu Valley, Tien Shan (Kyrgyzstan), based on 10Be surface exposure dating. Quat. Res. 77 (2), 281–288.
Zech, R., Abramowski, U., Glaser, B., Sosin, P., Kubik, P.W., Zech, W., 2005. Late Quaternary glacial and climate history of the Pamir Mountains derived from cosmogenic 10Be exposure ages. Quat. Res. 64 (2), 212–220.